Biomolecules & Biomedicine

RESEARCH ARTICLE

S-palmitoylation-related genes in Crohn's disease: Bioinformatic identification and validation

Yuyan Zhou [1] and Yuxuan Zhao [2*]

Crohn's disease (CD) is a complex chronic inflammatory bowel disorder characterized by the absence of reliable biomarkers and effective targeted treatments. Recent evidence has suggested a role for S-palmitoylation, a reversible post-translational modification, in immune regulation and intestinal inflammation. However, a systematic, gene-centric investigation explicitly linking S-palmitoylation to the pathogenesis and diagnosis of CD has not been conducted. To address this gap, our study employs a comprehensive bioinformatic analysis to identify and validate key genes associated with both CD and S-palmitoylation, assessing their potential as diagnostic biomarkers and therapeutic targets. Utilizing data from the Gene Expression Omnibus (GEO, GSE83448) and GeneCards, we identified 23 S-palmitoylation-associated differentially expressed genes in CD. Functional enrichment analysis indicated their significant roles in cysteine-specific S-palmitoylation and immunometabolic regulation. We applied machine learning algorithms, including least absolute shrinkage and selection operator regression and support vector machine-recursive feature elimination, to select nine hub genes. Validation in two independent cohorts (GSE16879 and GSE59071) and receiver operating characteristic analysis confirmed *ZDHHC23* and *IFITM1* as biomarkers with high diagnostic value. These genes also exhibited correlations with immune infiltration patterns, as determined by cell-type identification by estimating relative subsets of RNA transcripts, MCPcounter, and QuanTIseq. *In vitro* experiments corroborated consistent changes in mRNA and protein expression for both *ZDHHC23* and *IFITM1*, reinforcing their involvement in CD. This study offers systematic insights into the functional roles of S-palmitoylation-related genes in CD, providing a novel theoretical foundation for the development of diagnostic and targeted therapeutic strategies.

Keywords: Crohn's disease, S-palmitoylation, ZDHHC23, IFITM1, immune infiltration, machine learning.

Introduction

Crohn's disease (CD) is a chronic and progressive inflammatory bowel disease (IBD) characterized by transmural inflammation that can affect any part of the gastrointestinal tract [1]. The chronic nature of the disease often leads to severe complications, including intestinal strictures, complex fistulas, and perforations, significantly impacting the patient's quality of life [2]. Currently, the primary treatment approach involves anti-*TNF*-α biologics to alleviate symptoms and slow disease progression [3]. However, approximately 40% of patients either do not respond initially or lose their response over time [4, 5]. Furthermore, long-term immunosuppressive therapy carries risks of infections, cancers, and other autoimmune-related side effects [4, 6], emphasizing the urgent need for new therapeutic targets.

Protein S-palmitoylation is a reversible post-translational modification catalyzed by palmitoyl acyltransferases (PATs), in which palmitic acid or other long-chain fatty acids are covalently attached to cysteine residues [7, 8]. This modification plays a critical role in regulating the membrane localization, stability, and signaling of proteins [9, 10]. It is implicated in various diseases, including cancer progression through the modulation of oncogenic signals, metabolic reprogramming, immune evasion, and the development of neurological dysfunctions [11–15]. Notably, emerging studies have indicated that many molecular pathways related to CD are regulated by S-palmitoylation [16, 17]. For instance, Zhang et al. [18] demonstrated that the NOD-like receptor family, pyrin domain containing 3 (*NLRP3*), undergoes post-translational palmitoylation by *ZDHHC5* at its Leucine-Rich Repeat domain, facilitating the assembly and activation of the NLRP3 inflammasome. Similarly, another study implicated *ZDHHC21*-mediated palmitoylation of Themis, which enhances its protein stability and promotes interactions with *SHP-1* and *Grb2*, leading to the modulation of early T-cell receptor signaling [19].

Despite these compelling associations that highlight the significance of S-palmitoylation in gut homeostasis and inflammation, current evidence remains fragmented. Previous research has primarily focused on individual genes or pathways, and a systematic, unbiased investigation of the entire S-palmitoylation machinery in the specific context of CD is entirely lacking. Additionally, the potential of S-palmitoylation-related genes as diagnostic biomarkers for CD remains unexplored.

[1]Department of Gastroenterology, Jinan Central Hospital, Jinan, China; [2]Department of Radiology, Qilu Hospital of Shandong University, Jinan, China.

*Correspondence to Yuxuan Zhao: zhaoyuxuan1026@163.com

DOI: 10.17305/bb.2025.13221

© 2025 Zhou and Zhao. This article is available under a Creative Commons License (Attribution 4.0 International, as described at https://creativecommons.org/licenses/by/4.0/).

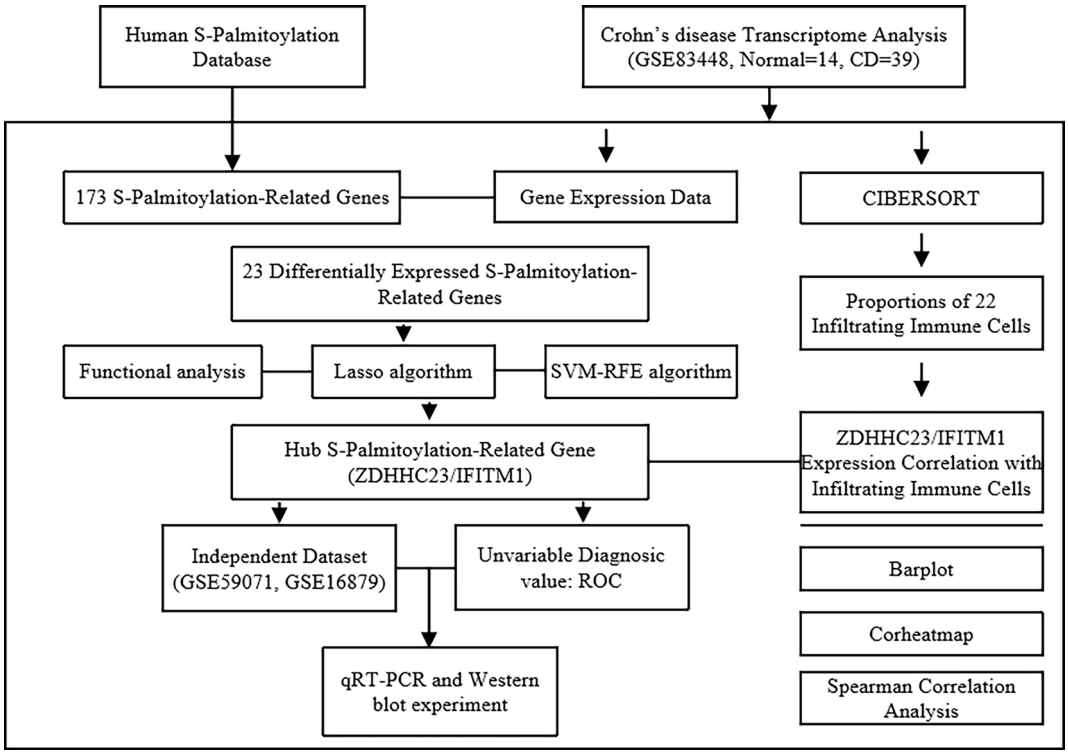

Figure 1. Flowchart of the study design. Genomic and transcriptomic data were extracted from the GEO database (GSE83448).

Therefore, this study aimed to investigate the dysregulation of S-palmitoylation-related genes in CD and to elucidate their diagnostic potential and immunological roles. To achieve this, we employed integrated bioinformatics approaches to identify and validate key genes, assess their diagnostic value, and determine their association with immune cell infiltration.

Materials and methods

Data acquisition and preprocessing

The gene expression microarray dataset GSE83448 was obtained from the National Center for Biotechnology Information Gene Expression Omnibus (NCBI GEO; https://www.ncbi.nlm.nih.gov/geo/) [20]. This discovery cohort comprised gene expression microarray profiles from intestinal mucosal biopsies of 39 CD patients and 14 healthy controls. Two independent validation cohorts (GSE16879 and GSE59071) were additionally retrieved to verify key findings. The workflow is illustrated in Figure 1.

Identification of S-palmitoylation-related differentially expressed genes (SP-DEGs)

Transcriptomic profiles from the GSE83448 dataset (CD vs healthy intestinal mucosal samples) were subjected to robust normalization and batch effect correction using the "limma" R package [21] (Figure S1). Differentially expressed genes (DEGs) were identified using standard exploratory thresholds of $|\log_2 \text{fold change}| > 0.3$ and an adjusted P value < 0.05 (Benjamini–Hochberg false discovery rate [FDR]). Data visualization included volcano plots and principal component analysis (PCA) generated via the "ggplot2" package. S-palmitoylation-related genes were systematically curated from the GeneCards database [22]. Intersection analysis between DEGs and palmitoylation-associated genes yielded SP-DEGs, visualized through Venn diagrams. Expression patterns of SP-DEGs were further illustrated by hierarchical clustering heatmaps and cohort-stratified boxplots.

Functional enrichment analysis of SP-DEGs

Functional enrichment analysis for SP-DEGs was performed using the Database for Annotation, Visualization, and Integrated Discovery (DAVID) Bioinformatics Database (https://davidbioinformatics.nih.gov/). This analysis encompassed three functional domains: biological process (BP), molecular function (MF), and cellular component (CC) [23]. Enriched terms were filtered by an FDR of <0.05 and visualized using the Xiantao Academic online platform (https://www.xiantaozi.com), which generated graphical representations including hierarchical bubble plots and circular ontology networks [24].

Machine learning-driven identification of CD hub genes

To optimize the candidate gene library, multi-stage feature selection was conducted on SP-DEGs from the GSE83448 cohort. Initially, least absolute shrinkage and selection operator (LASSO) regression was employed using the "glmnet" package. The optimal regularization parameter (λ) was determined through 10-fold cross-validation, selecting the value of lambda.min that minimized the mean cross-validated error. This L1 penalty term effectively shrank the coefficients of non-informative genes to zero, achieving dimensionality reduction and model parsimony [25, 26]. Concurrently, support vector machine-recursive feature elimination (SVM-RFE) was

performed [27]. SVM-RFE utilized a linear kernel with a cost parameter (*C*) of 1, with all features standardized to Z-scores prior to model training. The process was initialized with a random seed of 1234 to ensure reproducibility. SVM-RFE identified 12 key genes from the initial 23 SP-DEGs. The algorithm, facilitated by the "e1071" and "caret" packages, recursively eliminated features and ranked gene importance [28, 29]. The optimal feature subset was identified as the set yielding the highest cross-validated accuracy during the recursive process. To ensure robustness and generalizability, the performance of both models was rigorously validated through a separate, independent 10-fold cross-validation procedure.

The results from these two machine learning approaches were integrated to minimize model error rates, yielding a preliminary core gene set. To further refine this set, the GOSemSim package was employed to conduct Friends analysis, a functional association assessment based on Gene Ontology (GO) semantic similarity [30]. This analysis quantified each gene's significance within functional networks and generated a ranked list. High-confidence core genes were subsequently screened based on functional importance scores and visualized using raincloud plots.

Validation of hub gene expression and receiver operating characteristic (ROC) analysis

The differential expression of key genes between CD and healthy intestinal mucosal samples was validated using the GSE16879 and GSE59071 datasets. ROC curves were generated using the pROC package to evaluate the diagnostic value of these hub genes in CD. The area under the curve (AUC) values, along with 95% confidence intervals (CIs), were calculated for each hub gene across all cohorts. Pairwise comparisons of AUCs between cohorts for each gene were performed using DeLong's test to assess the consistency of diagnostic performance. The optimal cut-off value for each gene in each cohort was determined by maximizing Youden's J index (Youden's J = sensitivity + specificity – 1). The positive predictive value (PPV) and negative predictive value (NPV) were computed based on the observed prevalence of CD within each respective cohort.

Immune infiltration profiling

The relative proportions of immune cell subsets in intestinal mucosal samples from CD patients and healthy controls (GSE83448 cohort) were quantified using the cell-type identification by estimating relative subsets of RNA transcripts (CIBERSORT), MCP-counter, and QuanTIseq algorithms [31–33]. Spearman's rank correlation test was employed to assess associations between immune cell infiltration levels and the expression patterns of hub genes. Data visualization, including heatmaps and correlation matrices, was performed using the ggplot2 package in R, revealing significant interactions between S-palmitoylation-associated genes and immunoregulatory cell populations.

Cell culture

HT-29 cells were obtained from the Cell Bank of the Chinese Academy of Sciences. The cell line was authenticated through short tandem repeat (STR) profiling and tested negative for mycoplasma contamination by the provider. Cells were maintained until reaching 80%–90% confluency before experimental procedures, as described in earlier research [34]. For subsequent experiments, HT-29 cells were stimulated with 1 μg/mL lipopolysaccharide (LPS) for 24 h prior to use. Untreated HT-29 cells served as the control group, providing a baseline for comparison against the LPS-stimulated experimental group. Data from all *in vitro* experiments (quantitative reverse transcription PCR [qRT-PCR] and Western blot) are presented as mean ± SD from three independent biological replicates, with qRT-PCR assays performed in technical duplicate.

qRT-PCR

Total RNA was isolated from HT-29 cells using the RNAfast200 Total RNA Extraction Kit (Fastagen, Shanghai, China). First-strand cDNA synthesis was conducted via reverse transcription with the SureScript™ First-Strand cDNA Synthesis Kit (GeneCopoeia, Rockville, MD, USA). Quantitative PCR (qPCR) analysis was performed using the LightCycler® 480 Real-Time PCR System (Roche, Basel, Switzerland). All primer sequences are provided in Table S1.

Western blot

Total proteins were extracted from cells using radioimmunoprecipitation assay (RIPA) buffer (Beyotime, China). Following bicinchoninic acid (BCA) quantification, equal amounts of protein were separated by SDS-PAGE and transferred to polyvinylidene difluoride (PVDF) membranes. Membranes were blocked with 5% bovine serum albumin (BSA) for 1 h at room temperature and subsequently incubated overnight at 4 °C with primary antibodies diluted as follows: *GAPDH* (1:4000, Proteintech), *ZDHHC23* (1:1000, Epigentek), and *IFITM1* (1:1000, Proteintech). After washing with Tris-buffered saline with Tween 20 (TBST) three times for 10 min each, membranes were incubated with horseradish peroxidase (HRP)-conjugated goat anti-rabbit IgG (1:6000, Proteintech) for 1 h at room temperature. Protein bands were visualized using enhanced chemiluminescence (ECL) and quantified with ImageJ (NIH, USA).

Statistical analysis

Statistical analyses were conducted using GraphPad Prism 10 and R software (v4.2.0). For comparisons between two groups, the appropriate statistical test (Student's *t*-test, Welch's *t*-test, or Mann–Whitney *U* test) was determined based on the results of the Shapiro–Wilk normality test and Levene's test for homogeneity of variances. A P value < 0.05 was considered statistically significant ($P < 0.05$, $^{*}P < 0.01$, $^{***}P < 0.001$, $^{****}P < 0.0001$).

For correlation analyses between hub genes and immune cell infiltration (derived from CIBERSORT, MCPcounter, and QuanTIseq), we applied the Benjamini–Hochberg FDR correction to account for multiple testing. Each set of gene–cell pairs within a specific algorithm and cohort was treated as an independent hypothesis family. Associations with an FDR-adjusted P value (q-value) < 0.05 were considered significant, as indicated by asterisks in the figures.

Results

Identification of SP-DEGs in CD

To elucidate the role of S-palmitoylation in CD, we analyzed transcriptomic profiles from the GSE83448 dataset, which includes 39 CD intestinal biopsies and 14 healthy controls. Differential expression analysis identified 3743 DEGs (1992 upregulated, 1751 downregulated; adjusted P value < 0.05, $|\log2FC| > 0.3$), with distinct separation between CD and control groups visualized through PCA (Figure 2A) and a volcano plot (Figure 2B).

From the GeneCards database, we curated 173 S-palmitoylation-related genes, including key regulators, such as *ZDHHC* family acyltransferases and acyl-protein thioesterase (*APT*)/palmitoyl-protein thioesterase (*PPT*) thioesterases. Intersection analysis revealed 23 overlapping genes (Figure 2C and Table S2), designated as SP-DEGs. Hierarchical clustering (Figure 2D) demonstrated coherent dysregulation patterns of these SP-DEGs across all samples, while boxplots confirmed significant expression differences between CD and controls (Figure 2E). This systematic approach highlights the potential involvement of dynamic S-palmitoylation in CD pathogenesis.

Functional enrichment analysis of SP-DEGs

Functional enrichment analysis of the 23 SP-DEGs revealed their predominant involvement in cysteine-specific S-palmitoylation machinery and immune-metabolic dysregulation in CD. BPs were significantly enriched in S-palmitoylation-related terms (GO:0018230) and lipoprotein metabolism (GO:0042157), suggesting a dual role of SP-DEGs in post-translational modification and lipid-mediated inflammatory signaling. MFs emphasized the centrality of S-palmitoyltransferase activity (GO:0019706), with five SP-DEGs encoding key enzymes such as *ZDHHC* family members, which catalyze cysteine palmitoylation of immune receptors and trafficking proteins. CCs localized these genes to critical signaling hubs, including membrane microdomains (GO:0098857) and immunological synapses (GO:0001772), implicating S-palmitoylation in the spatial regulation of pro-inflammatory signaling complexes (Figure 3A–3D). Collectively, these results underscore a cohesive network where dysregulated S-palmitoylation dynamically modulates membrane protein localization, enzymatic activity, and immune cell communication in CD pathogenesis.

Identification of the S-palmitoylation hub genes in CD

To investigate the coordinated regulation among the SP-DEGs, we first performed co-expression network analysis, revealing tightly clustered interaction modules (Figure 4A). Subsequently, dual feature selection was conducted using LASSO regression and SVM-RFE algorithms. LASSO regression employed L1 regularization to minimize coefficients of non-critical variables, identifying 11 candidate core genes for CD (Figure 4B and 4C). Concurrently, the SVM-RFE algorithm selected 12 candidate core genes through iterative feature weight optimization (Figure 4D). Venn diagram analysis revealed nine consensus candidate core genes shared by both algorithms: *ZDHHC9*, *ZDHHC17*, *IFITM1*, *ZDHHC23*, *IGF2R*, *LAMP2*, *RHEB*, *JAM3*, and *ACSL5* (Figure 4E). Finally, Friends analysis prioritized these genes by importance ranking, leading to subsequent experimental validation (Figure 4F).

Multi-cohort validation of S-palmitoylation hub gene in CD

The expression patterns of nine hub genes were initially examined in the discovery cohort (GSE83448) and subsequently validated in two independent external cohorts (GSE16879 and GSE59071). This analysis revealed a significant downregulation of *ZDHHC23* ($P < 0.001$) and a marked upregulation of *IFITM1* ($P < 0.001$) in CD patients compared to controls (Figure 5A and 5B, Figure S2, and Table S3). ROC analysis demonstrated the excellent diagnostic capacity of the hub genes for CD. Specifically, *ZDHHC23* achieved an AUC of 0.956 (95% CI: 0.864–1.000) in the GSE16879 validation cohort. Overall, all hub genes maintained AUCs above 0.80 across independent cohorts (Figure 5C and 5D and Table S4). Pairwise comparisons using DeLong's test revealed no statistically significant differences in AUC values between cohorts for any hub gene (all $P > 0.05$, Table S5), supporting consistent diagnostic performance across diverse patient populations.

Analysis of immune cell infiltration

Using three deconvolution algorithms (CIBERSORT, MCP-counter, and QuanTIseq), we conducted an immune infiltration analysis on the GSE83448 dataset. To account for false positives due to multiple comparisons, all correlation analyses underwent Benjamini–Hochberg FDR correction, with a q-value < 0.05 considered statistically significant. Correlation matrix analysis identified the strongest negative interaction between resting natural killer (NK) cells and activated NK cells (Figure 6A–6F).

After FDR correction, *ZDHHC23* expression maintained a significant positive correlation with regulatory T cells (Tregs) and significant negative correlations with pro-inflammatory M0 macrophages and activated dendritic cells ($q < 0.05$; Figure 6G). Conversely, for *IFITM1*, only its positive correlation with T follicular helper cells and negative correlation with Tregs remained significant after FDR correction ($q < 0.05$; Figure 6H and Table S6). The correlation landscape for *ZDHHC23* across a broader panel of 12 immune subsets is detailed in Figure S3, indicating FDR-significant associations. A similar comprehensive analysis for *IFITM1* (Figure S4) revealed that, after FDR correction, its correlations with other immune cell types (including naive B cells, $CD8^+$ T cells, and M0 macrophages) were not statistically significant (all $q \geq 0.05$). These findings imply that *ZDHHC23* and *IFITM1* may constitute a counter-regulatory axis in CD, where lower *ZDHHC23* levels are associated with reduced immune tolerance, while higher *IFITM1* levels correlate with amplified effector T-cell responses.

Biological validation of hub genes

To further validate our findings, we established an *in vitro* model of CD using LPS-stimulated HT-29 cells. qRT-PCR and Western blot analyses were conducted to assess expression changes in the key genes *ZDHHC23* and *IFITM1*. Results indicated significantly reduced mRNA expression levels of *ZDHHC23* and

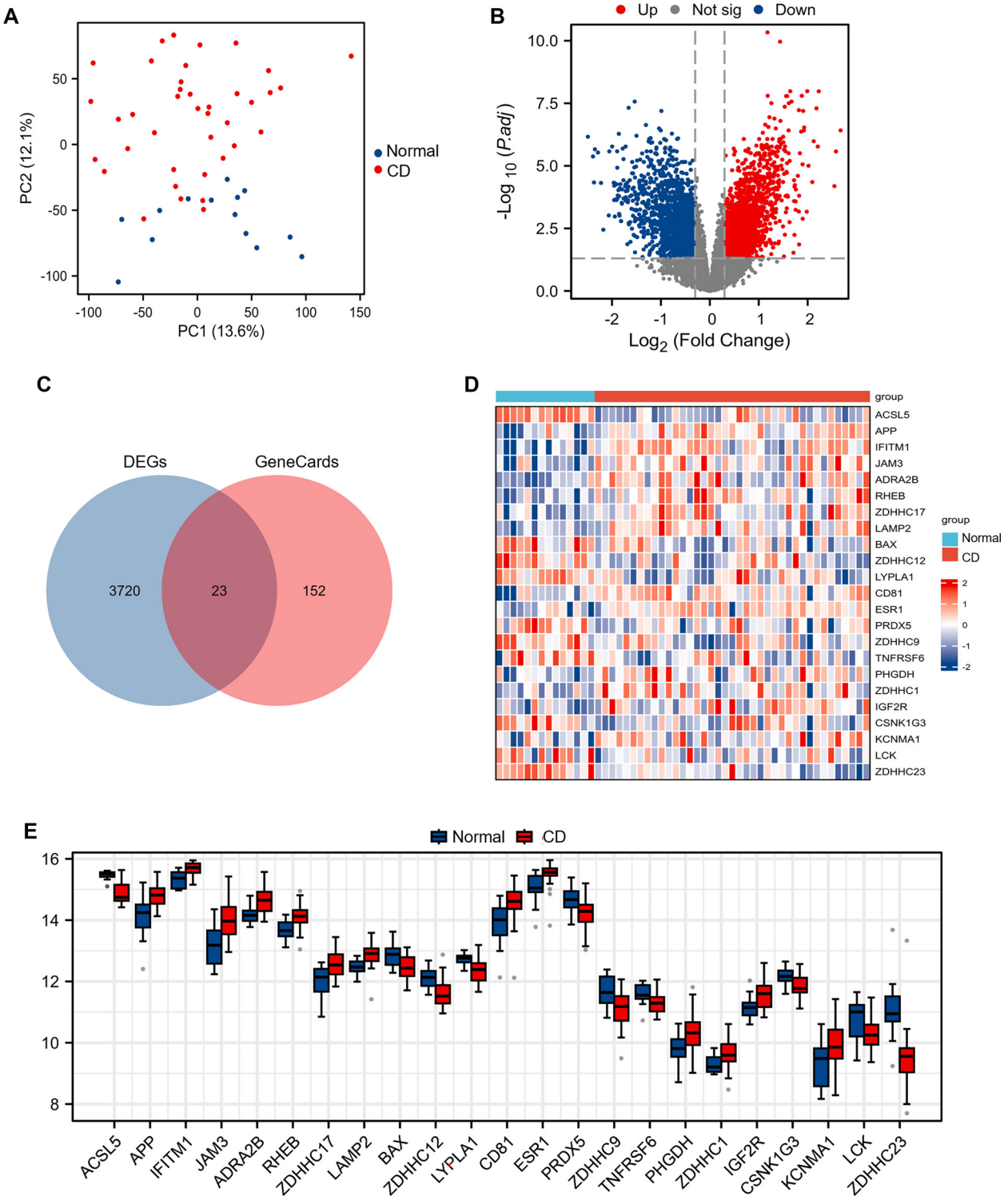

Figure 2. Differentially expressed S-palmitoylation-related genes in 39 CD intestinal biopsies and 14 healthy controls. (A) PCA for GSE83448. (B) Volcano plot illustrating 3743 DEGs. (C) Venn diagram depicting the overlap between DEGs and S-palmitoylation-related genes. (D) Heatmap representing the 23 SP-DEGs in CD and healthy controls. (E) Boxplots comparing the 23 SP-DEGs in CD and healthy controls. Abbreviations: CD: Crohn's disease; PCA: Principal component analysis; DEGs: Differentially expressed genes; SP-DEGs: S-palmitoylation-related differentially expressed genes.

markedly elevated expression of *IFITM1* in LPS-treated groups compared to controls (Figure 7A and 7B). Western blot analysis corroborated these findings, revealing corresponding trends of downregulation in ZDHHC23 protein and upregulation in IFITM1 protein (Figure 7C–7E). These observations align with our prior analytical conclusions and suggest that the downregulation of ZDHHC23 and upregulation of IFITM1 may contribute to the pathogenesis of CD.

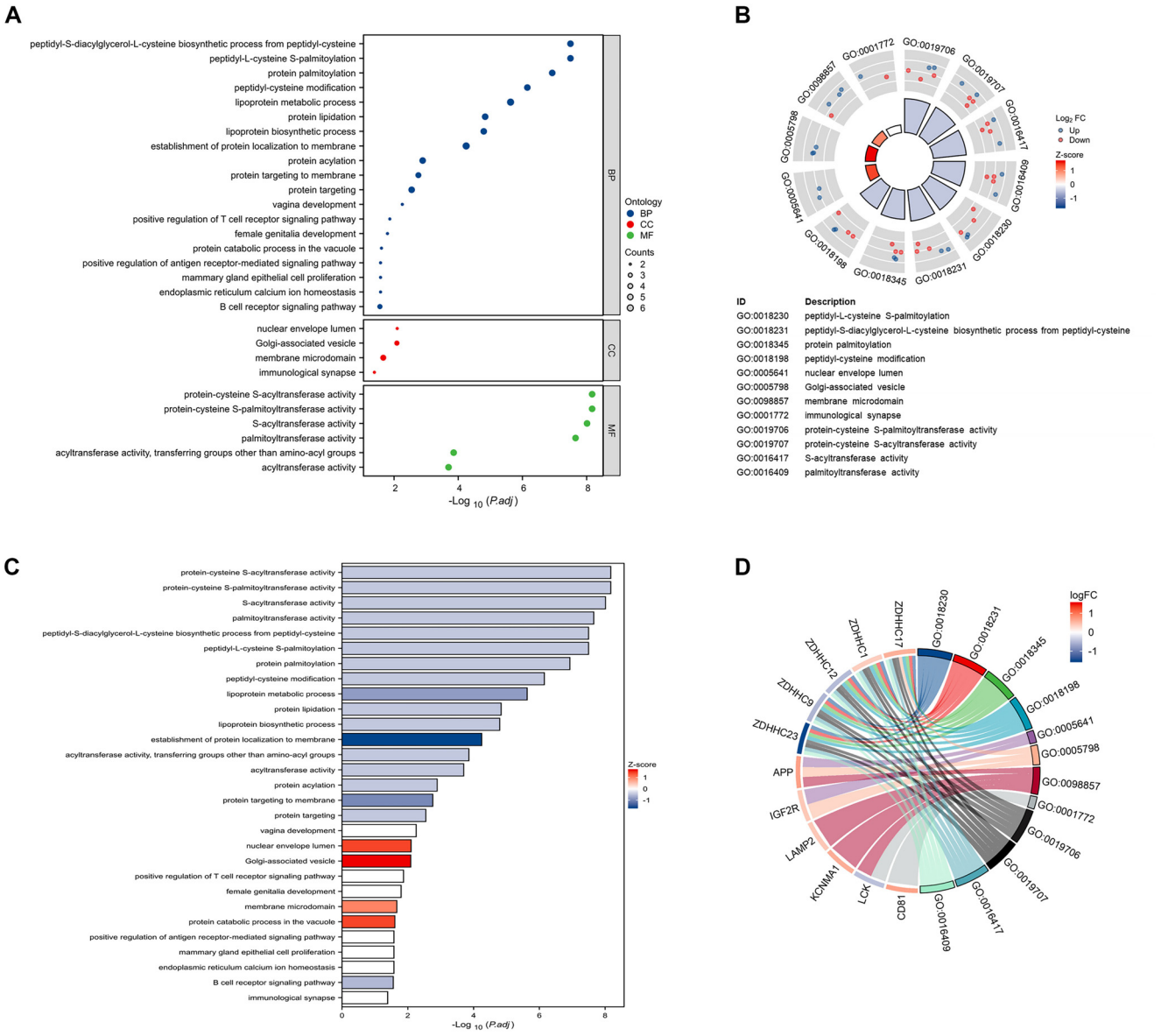

Figure 3. Functional enrichment analysis of SP-DEGs in the GSE83448 dataset. (A) The bubble plot illustrates key enriched terms across various categories. BP denotes biological processes; CC indicates cellular components; and MF represents molecular functions. (B) The circle map emphasizes BPs associated with S-palmitoylation. (C) The bar plot presents the results of the functional enrichment analysis, ranked by statistical significance. (D) The Circos plot visualizes the functional associations across categories. Abbreviations: SP-DEGs: S-palmitoylation-related differentially expressed genes; BP: Biological process; CC: Cellular component; MF: Molecular function.

Discussion

This study integrates bioinformatics and machine learning approaches to elucidate the role of S-palmitoylation in CD, identifying *ZDHHC23* and *IFITM1* as central regulatory hubs that connect post-translational modifications to immune-metabolic dysregulation. Both biomarkers exhibited consistent diagnostic performance across multiple independent cohorts, with their clinical potential bolstered by a comprehensive ROC analysis encompassing sensitivity, specificity, PPV, and NPV. Our findings not only enhance the understanding of CD pathogenesis but also propose novel therapeutic targets for this challenging condition.

The identification of 23 SP-DEGs underscores the critical role of dynamic lipid modifications in CD. Functional enrichment analysis indicates that these genes are primarily involved in immune synapse organization (GO:0001772) and lipoprotein metabolism (GO:0042157), which align with the dual pathological features of CD: chronic inflammation and metabolic reprogramming [35, 36]. Notably, the downregulation of *ZDHHC23* implies a disruption in the palmitoylation of immune receptors or barrier integrity proteins. This is consistent with prior evidence that impaired S-palmitoylation exacerbates mucosal inflammation by destabilizing tight junctions and enhancing nuclear factor kappa B (NF-κB) signaling [37–39].

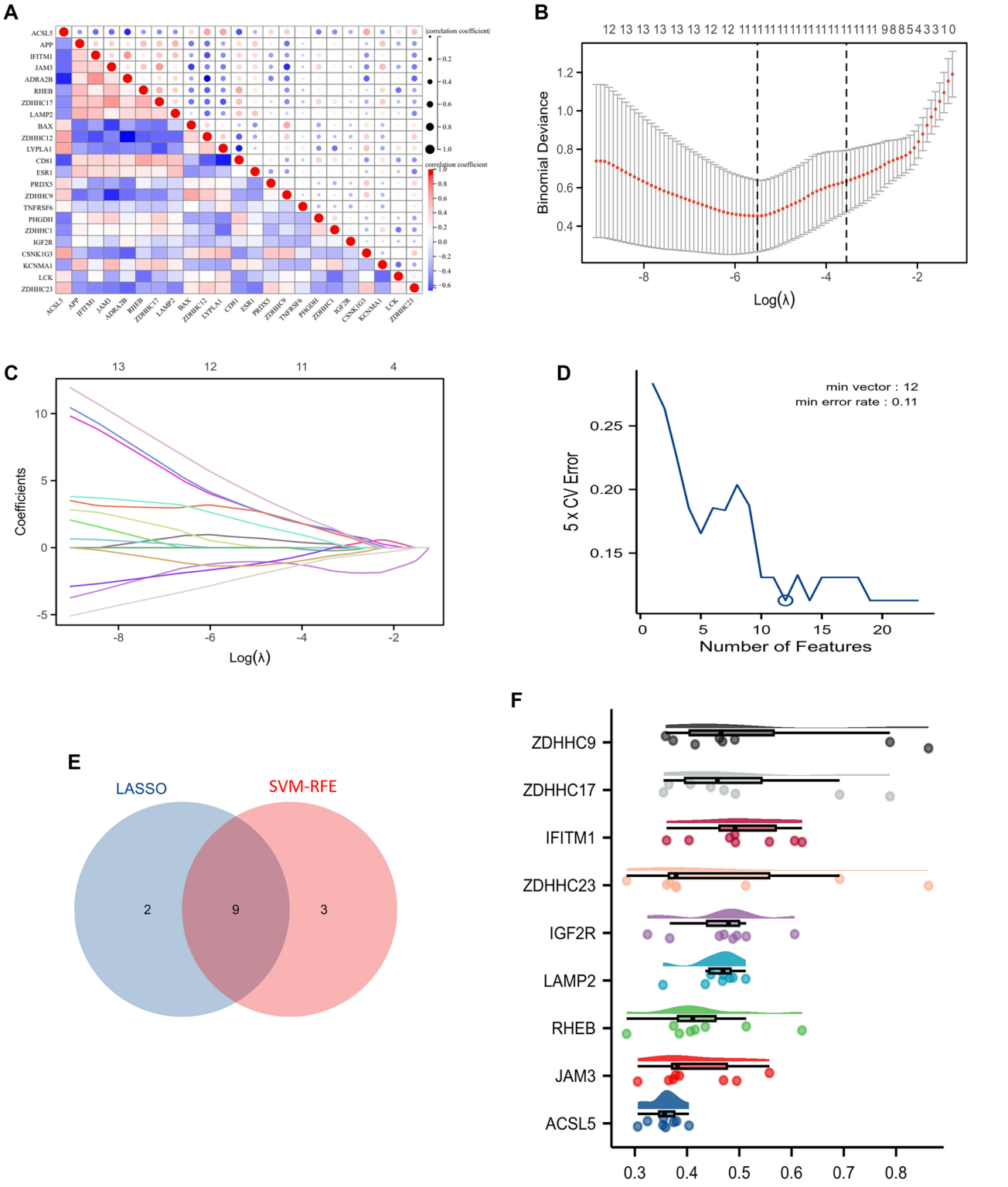

Figure 4. Identification of S-palmitoylation hub genes in CD. (A) Spearman's correlation analysis of the 23 SP-DEGs. (B and C) Eleven candidate biomarker genes were selected from the 23 potential hub genes using the LASSO algorithm. (D) Twelve candidate biomarker genes were identified from the 23 potential hub genes using the SVM-RFE algorithm. (E) The intersection revealed nine genes common to both machine learning algorithms. (F) Raincloud plots illustrate the similarity among the nine genes compared to other genes. Abbreviations: CD: Crohn's disease; SP-DEGs: S-palmitoylation-related differentially expressed genes; LASSO: Least absolute shrinkage and selection operator; SVM-RFE: Support vector machine-recursive feature elimination.

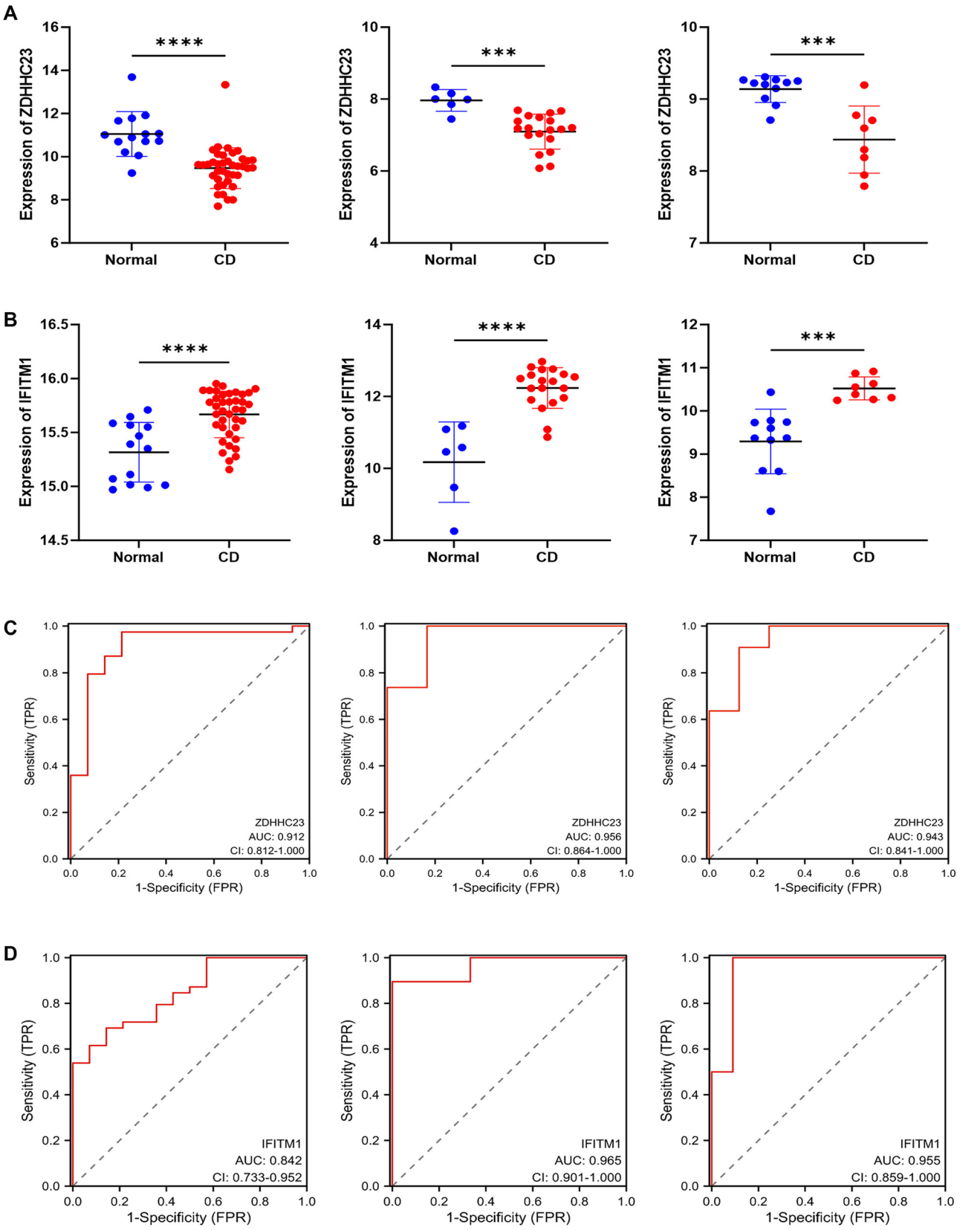

Figure 5. Multi-cohort validation of *ZDHHC23* and *IFITM1* as diagnostic biomarkers for CD. (A) Significant downregulation of *ZDHHC23* expression across multiple CD cohorts. (B) Significant upregulation of *IFITM1* expression across multiple CD cohorts. (C) ROC curve illustrating the diagnostic utility of *ZDHHC23* in CD detection. (D) ROC curve illustrating the diagnostic utility of *IFITM1* in CD detection. Asterisks indicate statistical significance (***$P < 0.001$; ****$P < 0.0001$). Abbreviations: CD: Crohn's disease; ROC: Receiver operating characteristic.

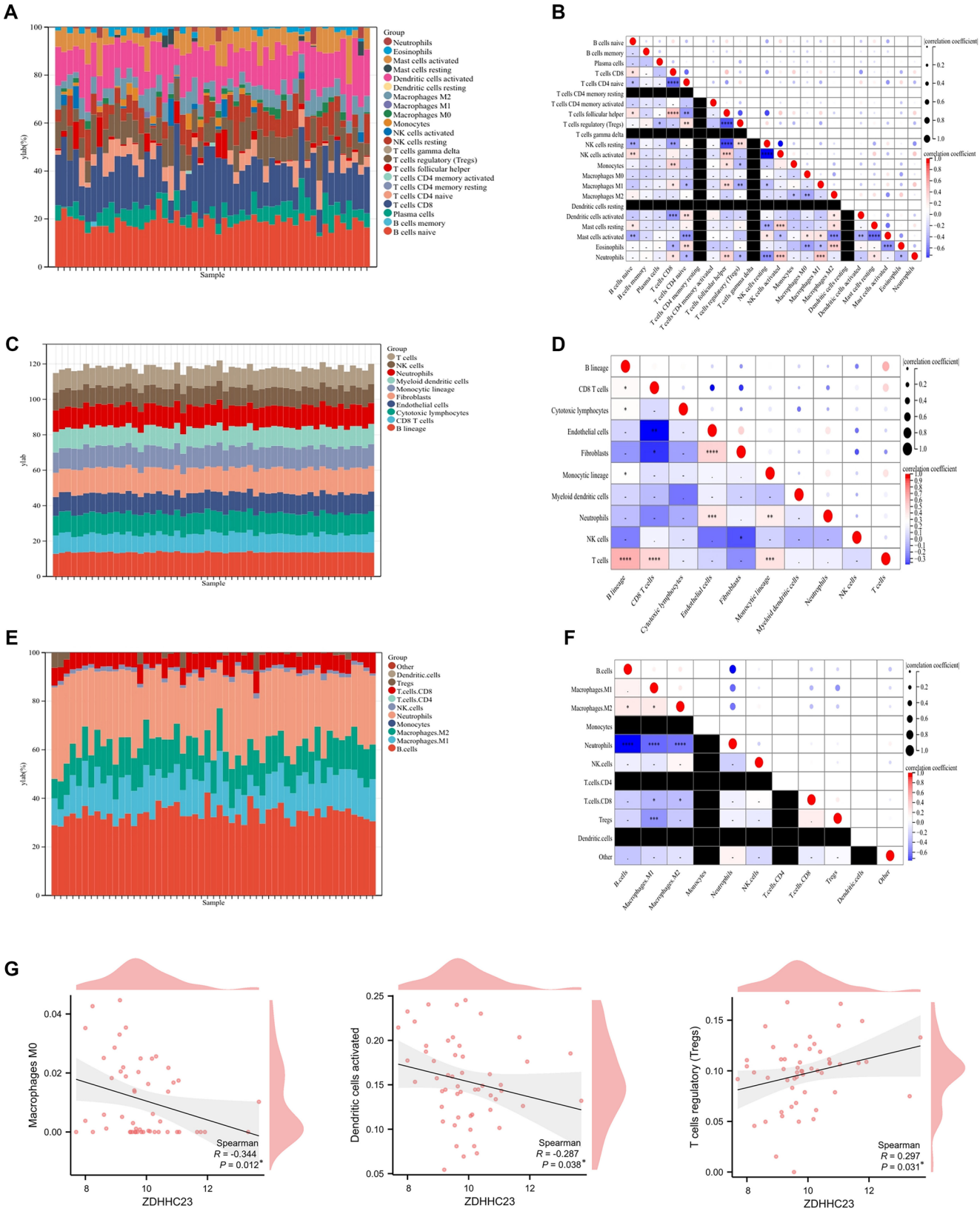

Figure 6. Continued on next page

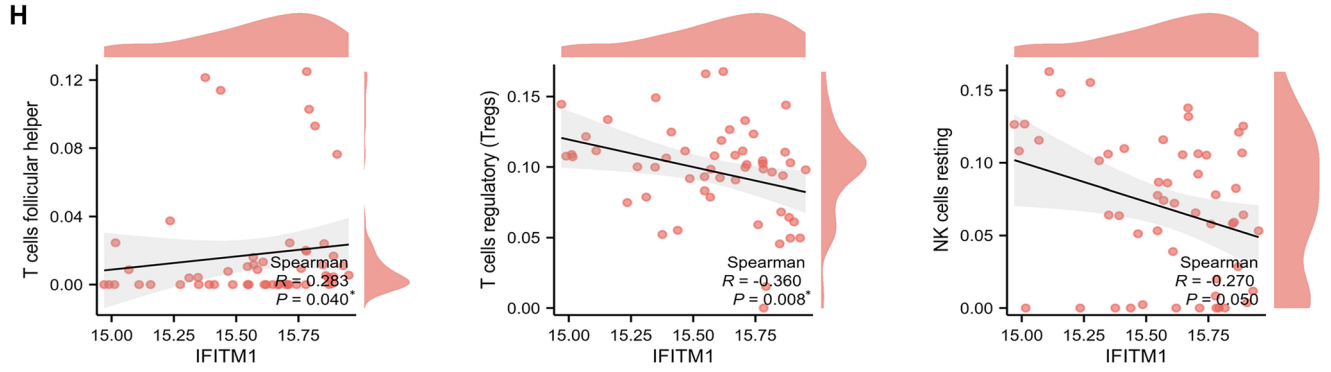

Figure 6. (Continued) Visualization of immune cell infiltration. (A and B) The correlation matrix of infiltrating immune cell composition and proportions was generated using the CIBERSORT algorithm. (C and D) The correlation matrix of infiltrating immune cell composition and proportions was produced using the MCPcounter algorithm. (E and F) The correlation matrix of infiltrating immune cell composition and proportions was established using the QuanTIseq algorithm. (G) Correlation between *ZDHHC23* expression and infiltrating immune cells, specifically M0 Macrophages, activated dendritic cells, and regulatory T cells. (H) Correlation between *IFITM1* expression and infiltrating immune cells, including follicular helper T cells, regulatory T cells, and resting NK cells. Asterisks (*) indicate correlations that remained statistically significant after FDR correction for multiple testing across all gene–cell pairs within each algorithm ($q < 0.05$). Abbreviations: CIBERSORT: Cell-type identification by estimating relative subsets of RNA transcripts; FDR: False discovery rate; NK: Natural killer.

The strong negative correlation between *ZDHHC23* and M0 macrophages further implicates its role in suppressing pro-inflammatory myeloid activation. Mechanistically, *ZDHHC23* may influence macrophage polarization by palmitoylating RAC1 or STAT3, both of which are critical for maintaining the M1/M2 balance [40–42]. While our study identifies *ZDHHC23* as a promising therapeutic target, we emphasize the necessity of functional validation through knockout models and compound screening prior to clinical translation. Conversely, its positive association with regulatory T cells (Tregs) suggests a protective role in sustaining immune tolerance, potentially through palmitoylation-dependent stabilization of FOXP3 or CTLA-4 [43–45]. These findings position S-palmitoylation as a rheostat that fine-tunes immune homeostasis in the gut. The consistent downregulation of *ZDHHC23* across discovery and validation cohorts (GSE83448 and GSE16879) and its high diagnostic accuracy (AUC > 0.85) underscore its clinical relevance. This parallels studies in cancer, where the loss of *ZDHHC23* drives metastasis through RAS depalmitoylation [46, 47], suggesting a conserved mechanism across inflammatory and neoplastic contexts. Notably, the dysregulation of *ZDHHC23* may account for the secondary failure of anti-TNF therapies in CD, as tumor necrosis factor-alpha (TNF-α) signaling requires the palmitoylation of TNFR1 for proper membrane localization [48]; decreased *ZDHHC23* activity could impair TNFR1 trafficking, reducing drug efficacy [49, 50]. Targeting *ZDHHC23* or its substrates may restore therapeutic responsiveness, providing a precision medicine approach for non-responders.

Furthermore, this study elucidates the dual role of *IFITM1* in CD, where its consistently elevated expression in CD patients and LPS-stimulated intestinal epithelial cells correlates positively with follicular helper T cells (Tfh). These findings suggest that *IFITM1* may enhance mucosal antibody responses by promoting Tfh-mediated B-cell activation, consistent with previous reports of *IFITM1* facilitating inflammasome activation in inflammatory contexts [51, 52]. The stable high AUC values across validation cohorts reflect IFITM1's sensitivity to intestinal inflammation, likely due to its classification as an interferon-stimulated gene (ISG) that undergoes synergistic induction by TNF-α and interferon-gamma (IFN-γ) within inflammatory microenvironments [53, 54]. Importantly, *IFITM1* is a confirmed palmitoylation substrate (Cys72/83/105), and its functional dynamics are dependent on modification status. Palmitoylation enhances IFITM1's localization to lipid rafts, facilitating its inhibition of viral membrane fusion [54]. In CD, while we observed increased IFITM1 protein levels, its palmitoylation efficiency requires further validation. Collectively, our results indicate that IFITM1's role in CD extends beyond conventional interferon effector functions.

Several limitations should be acknowledged when interpreting our results. First, the use of non-nested cross-validation in our machine learning feature selection may introduce optimistic bias in performance estimates. Although we employed independent validation cohorts to mitigate this concern, future studies would benefit from nested cross-validation frameworks for more robust performance metrics. Second, the association between *ZDHHC23*/*IFITM1* and immune dysregulation remains correlative; *in vitro* experiments, such as CRISPR-Cas9 knockdown in intestinal organoids, are necessary to validate the functional impact on barrier integrity and cytokine production. Third, bulk RNA-seq data from mucosal biopsies may obscure cell-type-specific palmitoylation dynamics, and single-cell sequencing could address spatial heterogeneity. Additionally, while our *in vitro* experiments utilized a sample size of $n = 3$ biological replicates, which is standard in the field, we acknowledge that this modest sample size warrants consideration. However, the consistency of our findings across both mRNA and protein levels, coupled with the significant effect sizes observed, lends confidence to the robustness of these results. Lastly, while PAT inhibition has been explored in cancer [55, 56], therapeutic translation for CD requires complementary approaches: developing *ZDHHC23*-targeted agonists to

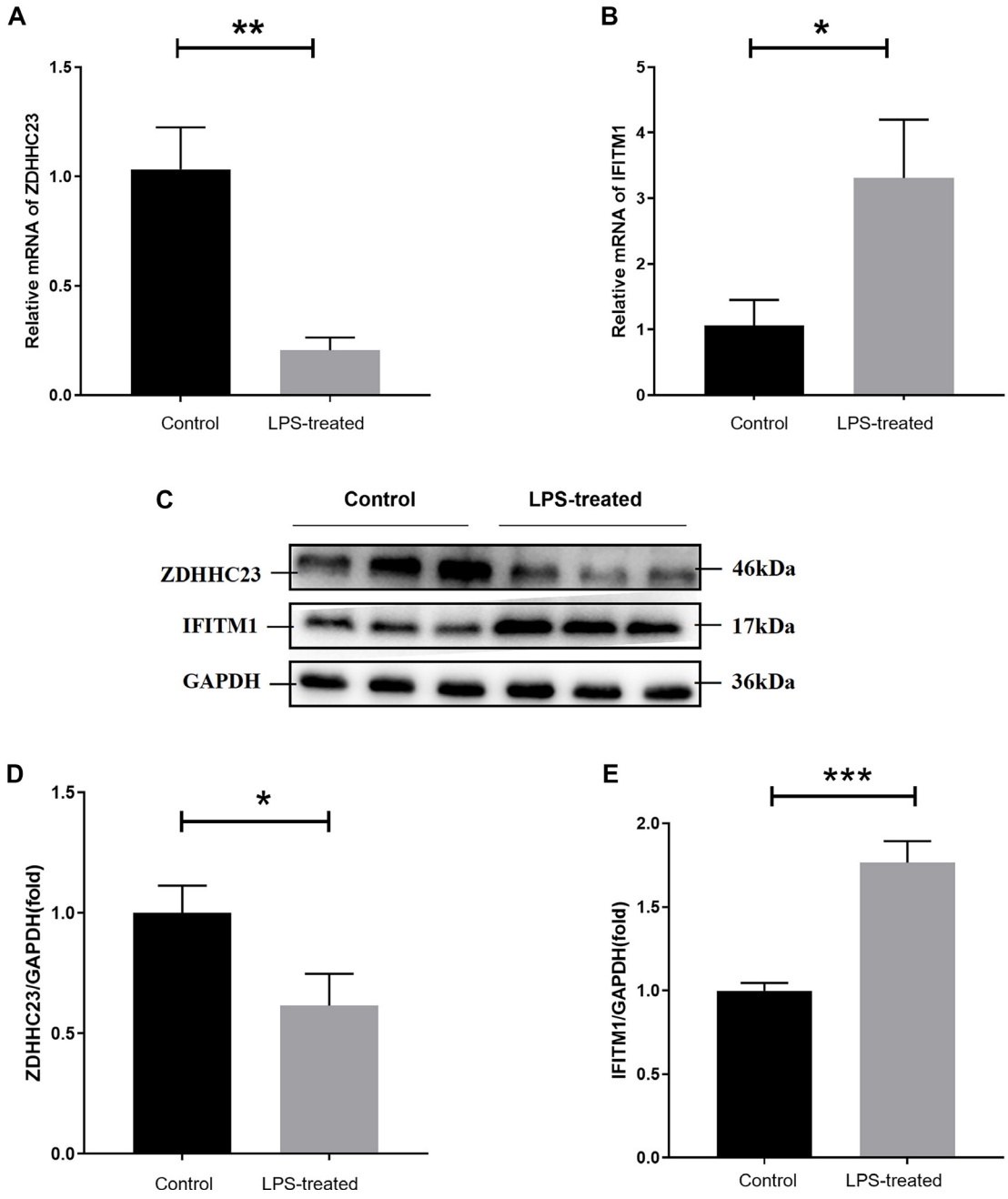

Figure 7. Experimental validation of *ZDHHC23* and *IFITM1* expression in LPS-treated HT-29 cells. The expression levels of *ZDHHC23* and *IFITM1* in HT-29 cells were validated through qRT-PCR analysis, which confirmed mRNA levels for *ZDHHC23* (A) and *IFITM1* (B). Western blot analysis (C) demonstrated protein expression differences between control and LPS-treated HT-29 cells ($n = 3$ biological replicates). Densitometric quantification of protein expression was performed for ZDHHC23 (D) and IFITM1 (E). Asterisks indicate statistical significance (*$P < 0.05$; **$P < 0.01$; ***$P < 0.001$). Abbreviations: LPS: Lipopolysaccharide; qRT-PCR: Quantitative reverse transcription PCR.

restore anti-inflammatory palmitoylation alongside IFITM1-neutralizing biologics to disrupt its membrane-associated pro-inflammatory pathways. Moreover, the strong diagnostic performance of both *ZDHHC23* and *IFITM1* supports their potential as clinical biomarkers for CD stratification and monitoring. Future work should address the challenges of developing specific palmitoylation-targeted therapies and validating these biomarkers in larger clinical cohorts to establish their definitive diagnostic and therapeutic utility.

Conclusion

This study systematically identifies SP-DEGs in CD through comprehensive bioinformatics analysis. Among these, *ZDHHC23* and *IFITM1* were established as hub biomarkers demonstrating consistent diagnostic value across multiple validation cohorts. Experimental validation confirmed their dysregulation at both transcriptional and protein levels, while immune infiltration analysis revealed significant correlations with specific immune cell subsets. These findings not only

provide novel insights into the molecular mechanisms of S-palmitoylation in CD pathogenesis but also offer potential biomarkers for diagnostic development and therapeutic targeting.

Conflicts of interest: Authors declare no conflicts of interest.

Funding: Authors received no specific funding for this work.

Data availability: The data that support the findings of this study are available in Gene Expression Omnibus (datasets with identifiers: GSE83448, GSE16879, and GSE59071), which were downloaded from http://www.ncbi.nlm.nih.gov/geo/.

Submitted: 06 September 2025
Accepted: 12 November 2025
Published online: 09 December 2025

References

[1] Sazonovs A, Stevens CR, Venkataraman GR, Yuan K, Avila B, Abreu MT, et al. Large-scale sequencing identifies multiple genes and rare variants associated with Crohn's disease susceptibility. Nat Genet 2022;54(9):1275–83. https://doi.org/10.1038/s41588-022-01156-2.

[2] Cao S, Colonna M, Deepak P. Pathogenesis of perianal fistulising Crohn's disease: current knowledge, gaps in understanding, and future research directions. J Crohns Colitis 2023;17(6):1010–22. https://doi.org/10.1093/ecco-jcc/jjad008.

[3] Gisbert JP, Chaparro M. Anti-TNF agents and new biological agents (vedolizumab and ustekinumab) in the prevention and treatment of postoperative recurrence after surgery in Crohn's disease. Drugs 2023;83(13):1179–205. https://doi.org/10.1007/s40265-023-01916-2.

[4] Zheng M, Han R, Yuan Y, Xing Y, Zhang W, Sun Z, et al. The role of Akkermansia muciniphila in inflammatory bowel disease: current knowledge and perspectives. Front Immunol 2022;13:1089600. https://doi.org/10.3389/fimmu.2022.1089600.

[5] Ding NS, Hart A, De Cruz P. Systematic review: predicting and optimising response to anti-TNF therapy in Crohn's disease—algorithm for practical management. Aliment Pharmacol Ther 2016;43(1):30–51. https://doi.org/10.1111/apt.13445.

[6] Foppa C, Rizkala T, Repici A, Hassan C, Spinelli A. Microbiota and IBD: current knowledge and future perspectives. Dig Liver Dis 2024;56(6):911–22. https://doi.org/10.1016/j.dld.2023.11.015.

[7] Mesquita FS, Abrami L, Linder ME, Bamji SX, Dickinson BC, van der Goot FG. Mechanisms and functions of protein S-acylation. Nat Rev Mol Cell Biol 2024;25(6):488–509. https://doi.org/10.1038/s41580-024-00700-8.

[8] Main A, Fuller W. Protein S-palmitoylation: advances and challenges in studying a therapeutically important lipid modification. FEBS J 2022;289(4):861–82. https://doi.org/10.1111/febs.15781.

[9] Zhang MM, Hang HC. Protein S-palmitoylation in cellular differentiation. Biochem Soc Trans 2017;45(1):275–85. https://doi.org/10.1042/bst20160236.

[10] Chen R, Tang X, Wang Y, Wang B, Mao F. Protein palmitoylation: an emerging regulator of inflammatory signaling and diseases. Front Immunol 2025;16:1652741. https://doi.org/10.3389/fimmu.2025.1652741.

[11] Das T, Yount JS, Hang HC. Protein S-palmitoylation in immunity. Open Biol 2021;11(3):200411. https://doi.org/10.1098/rsob.200411.

[12] Li P, Gong X, Yuan L, Mu L, Zheng Q, Xiao H, et al. Palmitoylation in apoptosis. J Cell Physiol 2023;238(8):1641–50. https://doi.org/10.1002/jcp.31047.

[13] Zhang Y, Qin Z, Sun W, Chu F, Zhou F. Function of protein S-palmitoylation in immunity and immune-related diseases. Front Immunol 2021;12:661202. https://doi.org/10.3389/fimmu.2021.661202.

[14] Pei S, Piao HL. Exploring protein S-palmitoylation: mechanisms, detection, and strategies for inhibitor discovery. ACS Chem Biol 2024;19(9):1868–82. https://doi.org/10.1021/acschembio.4c00110.

[15] De I, Sadhukhan S. Emerging roles of DHHC-mediated protein S-palmitoylation in physiological and pathophysiological context. Eur J Cell Biol 2018;97(5):319–38. https://doi.org/10.1016/j.ejcb.2018.03.005.

[16] Cheng WX, Ren Y, Lu MM, Xu LL, Gao JG, Chen D, et al. Palmitoylation in Crohn's disease: current status and future directions. World J Gastroenterol 2021;27(48):8201–15. https://doi.org/10.3748/wjg.v27.i48.8201.

[17] Li H, Yuan Q, Wang S, Yu T, Qi X. Role of S-palmitoylation in digestive system diseases. Cell Death Discov 2025;11(1):331. https://doi.org/10.1038/s41420-025-02629-z.

[18] Zheng S, Que X, Wang S, Zhou Q, Xing X, Chen L, et al. ZDHHC5-mediated NLRP3 palmitoylation promotes NLRP3-NEK7 interaction and inflammasome activation. Mol Cell 2023;83(24):4570–85.e7. https://doi.org/10.1016/j.molcel.2023.11.015.

[19] Meng C, Dai X, Sun L, Huang D, Xu X, Cheng Y, et al. ZDHHC21-driven S-palmitoylation of Themis regulates the function of T cells and maintains homeostatic balance. Cell Commun Signal 2025;23(1):401. https://doi.org/10.1186/s12964-025-02396-5.

[20] Barrett T, Wilhite SE, Ledoux P, Evangelista C, Kim IF, Tomashevsky M, et al. NCBI GEO: archive for functional genomics data sets–update. Nucl Acids Res 2013;41:D991–5. https://doi.org/10.1093/nar/gks1193.

[21] Liu S, Wang Z, Zhu R, Wang F, Cheng Y, Liu Y. Three differential expression analysis methods for RNA sequencing: limma, EdgeR, DESeq2. J Vis Exp 2021;(175):62528. https://doi.org/10.3791/62528.

[22] Safran M, Dalah I, Alexander J, Rosen N, Iny Stein T, Shmoish M, et al. GeneCards version 3: the human gene integrator. Database (Oxford) 2010;2010:baq020. https://doi.org/10.1093/database/baq020.

[23] Sherman BT, Hao M, Qiu J, Jiao X, Baseler MW, Lane HC, et al. DAVID: a web server for functional enrichment analysis and functional annotation of gene lists (2021 update). Nucl Acids Res 2022;50(W1):W216–21. https://doi.org/10.1093/nar/gkac194.

[24] Tang L, Chen J, Wu Z, Wang L, Lai Y, Chen Z, et al. FUNDC1 predicts poor prognosis and promotes progression and chemoresistance in endometrial carcinoma. J Cancer 2024;15(20):6490–504. https://doi.org/10.7150/jca.96877.

[25] Ali H, Shahzad M, Sarfraz S, Sewell KB, Alqalyoobi S, Mohan BP. Application and impact of Lasso regression in gastroenterology: A systematic review. Indian J Gastroenterol 2023;42(6):780–90. https://doi.org/10.1007/s12664-023-01426-9.

[26] Wang L, Wu P, Liu Y, Patel DC, Leonard TB, Zhao H. Clustering-aided prediction of outcomes in patients with idiopathic pulmonary fibrosis. Respir Res 2024;25(1):383. https://doi.org/10.1186/s12931-024-03015-6.

[27] Sanz H, Valim C, Vegas E, Oller JM, Reverter F. SVM-RFE: selection and visualization of the most relevant features through non-linear kernels. BMC Bioinformatics 2018;19(1):432. https://doi.org/10.1186/s12859-018-2451-4.

[28] Lu H, Lan S, Yuan X, Li P. Functional enrichment, drug prediction, and molecular docking to identify fibroblast-related biomarkers for gastric cancer via high-dimensional weighted gene co-expression network analysis. Endocr Metab Immune Disord Drug Targets Online ahead of print. https://doi.org/10.2174/0118715303424481250929070902.

[29] Wang Z, Zhang Z. Biomarkers associated with cell-in-cell structure in kidney renal clear cell carcinoma based on transcriptome sequencing. PeerJ 2025;13:e19246. https://doi.org/10.7717/peerj.19246.

[30] Yu G, Li F, Qin Y, Bo X, Wu Y, Wang S. GOSemSim: an R package for measuring semantic similarity among GO terms and gene products. Bioinformatics 2010;26(7):976–8. https://doi.org/10.1093/bioinformatics/btq064.

[31] Newman AM, Liu CL, Green MR, Gentles AJ, Feng W, Xu Y, et al. Robust enumeration of cell subsets from tissue expression profiles. Nat Methods 2015;12(5):453–7. https://doi.org/10.1038/nmeth.3337.

[32] Helmink BA, Reddy SM, Gao J, Zhang S, Basar R, Thakur R, et al. B cells and tertiary lymphoid structures promote immunotherapy response. Nature 2020;577(7791):549–55. https://doi.org/10.1038/s41586-019-1922-8.

[33] Finotello F, Mayer C, Plattner C, Laschober G, Rieder D, Hackl H, et al. Molecular and pharmacological modulators of the tumor immune contexture revealed by deconvolution of RNA-seq data. Genome Med 2019;11(1):34. https://doi.org/10.1186/s13073-019-0638-6.

[34] Bruckner RS, Spalinger MR, Barnhoorn MC, Feakins R, Fuerst A, Jehle EC, et al. Contribution of CD3+CD8− and CD3+CD8+ T Cells to TNF-alpha overexpression in Crohn disease-associated perianal fistulas and induction of epithelial-mesenchymal transition in HT-29

cells. Inflamm Bowel Dis 2021;27(4):538–49. https://doi.org/10.1093/ibd/izaa240.
[35] Pan X, Zhu Q, Pan LL, Sun J. Macrophage immunometabolism in inflammatory bowel diseases: from pathogenesis to therapy. Pharmacol Ther 2022;238:108176. https://doi.org/10.1016/j.pharmthera.2022.108176.
[36] Adolph TE, Meyer M, Schwarzler J, Mayr L, Grabherr F, Tilg H. The metabolic nature of inflammatory bowel diseases. Nat Rev Gastroenterol Hepatol 2022;19(12):753–67. https://doi.org/10.1038/s41575-022-00658-y.
[37] Aramsangtienchai P, Spiegelman NA, Cao J, Lin H. S-Palmitoylation of junctional adhesion molecule C regulates its tight junction localization and cell migration. J Biol Chem 2017;292(13):5325–34. https://doi.org/10.1074/jbc.m116.730523.
[38] Oda Y, Sugawara T, Fukata Y, Izumi Y, Otani T, Higashi T, et al. The extracellular domain of angulin-1 and palmitoylation of its cytoplasmic region are required for angulin-1 assembly at tricellular contacts. J Biol Chem 2020;295(13):4289–302. https://doi.org/10.1074/jbc.ra119.010491.
[39] Zingler P, Sarchen V, Glatter T, Caning L, Saggau C, Kathayat RS, et al. Palmitoylation is required for TNF-R1 signaling. Cell Commun Signal 2019;17(1):90. https://doi.org/10.1186/s12964-019-0405-8.
[40] Feng Z, Meng F, Huo F, Zhu Y, Qin Y, Gui Y, et al. Inhibition of ferroptosis rescues M2 macrophages and alleviates arthritis by suppressing the HMGB1/TLR4/STAT3 axis in M1 macrophages. Redox Biol 2024;75:103255. https://doi.org/10.1016/j.redox.2024.103255.
[41] Fan X, Zhang S, Sun S, Bi W, Li S, Wang W, et al. GFAP palmitoylation mediated by ZDHHC23 in spinal astrocytes contributes to the development of neuropathic pain. Reg Anesth Pain Med 2024;49(11):821–30. https://doi.org/10.1136/rapm-2023-104980.
[42] Dai T, Zhao Z, Zhu T, Fei C, Nie L, Chen J. The anti-inflammatory role of zDHHC23 through the promotion of macrophage M2 polarization and macrophage necroptosis in large yellow croaker (Larimichthys crocea). Front Immunol 2024;15:1401626. https://doi.org/10.3389/fimmu.2024.1401626.
[43] Barbi J, Pardoll D, Pan F. Treg functional stability and its responsiveness to the microenvironment. Immunol Rev 2014;259(1):115–39. https://doi.org/10.1111/imr.12172.
[44] Wang K, Fu W. Transcriptional regulation of Treg homeostasis and functional specification. Cell Mol Life Sci 2020;77(21):4269–87. https://doi.org/10.1007/s00018-020-03534-7.
[45] Tekguc M, Wing JB, Osaki M, Long J, Sakaguchi S. Treg-expressed CTLA-4 depletes CD80/CD86 by trogocytosis, releasing free PD-L1 on antigen-presenting cells. Proc Natl Acad Sci U S A 2021;118(30):e2023739118. https://doi.org/10.1073/pnas.2023739118.
[46] Mitchell DA, Hamel LD, Reddy KD, Farh L, Rettew LM, Sanchez PR, et al. Mutations in the X-linked intellectual disability gene, zDHHC9, alter autopalmitoylation activity by distinct mechanisms. J Biol Chem 2014;289(26):18582–92. https://doi.org/10.1074/jbc.m114.567420.
[47] Mitchell DA, Vasudevan A, Linder ME, Deschenes RJ. Protein palmitoylation by a family of DHHC protein S-acyltransferases. J Lipid Res 2006;47(6):1118–27. https://doi.org/10.1194/jlr.r600007-jlr200.
[48] Poggi M, Kara I, Brunel JM, Landrier JF, Govers R, Bonardo B, et al. Palmitoylation of TNF alpha is involved in the regulation of TNF receptor 1 signalling. Biochim Biophys Acta 2013;1833(3):602–12. https://doi.org/10.1016/j.bbamcr.2012.11.009.
[49] Souza RF, Caetano MAF, Magalhaes HIR, Castelucci P. Study of tumor necrosis factor receptor in the inflammatory bowel disease. World J Gastroenterol 2023;29(18):2733–46. https://doi.org/10.3748/wjg.v29.i18.2733.
[50] Waschke KA, Villani AC, Vermeire S, Dufresne L, Chen TC, Bitton A, et al. Tumor necrosis factor receptor gene polymorphisms in Crohn's disease: association with clinical phenotypes. Am J Gastroenterol 2005;100(5):1126–33. https://doi.org/10.1111/j.1572-0241.2005.40534.x.
[51] Han J, Wu M, Liu Z. Dysregulation in IFN-gamma signaling and response: the barricade to tumor immunotherapy. Front Immunol 2023;14:1190333. https://doi.org/10.3389/fimmu.2023.1190333.
[52] Song L, Wang D, Abbas G, Li M, Cui M, Wang J, et al. The main protease of SARS-CoV-2 cleaves histone deacetylases and DCP1A, attenuating the immune defense of the interferon-stimulated genes. J Biol Chem 2023;299(3):102990. https://doi.org/10.1016/j.jbc.2023.102990.
[53] Nguyen HM, Gaikwad S, Oladejo M, Agrawal MY, Srivastava SK, Wood LM. Interferon stimulated gene 15 (ISG15) in cancer: an update. Cancer Lett 2023;556:216080. https://doi.org/10.1016/j.canlet.2023.216080.
[54] Shi X, Chen S, Liu M, Fan Y, Wen X, Wang J, et al. The unconventional role of ABHD17A in increasing the S-palmitoylation and antiviral activity of IFITM1 by downregulating ABHD16A. Biomolecules 2025;15(7):992. https://doi.org/10.3390/biom15070992.
[55] Wang Y, Shen N, Yang Y, Xia Y, Zhang W, Lu Y, et al. ZDHHC5-mediated S-palmitoylation of FAK promotes its membrane localization and epithelial-mesenchymal transition in glioma. Cell Commun Signal 2024;22(1):46. https://doi.org/10.1186/s12964-023-01366-z.
[56] Zhou B, Hao Q, Liang Y, Kong E. Protein palmitoylation in cancer: molecular functions and therapeutic potential. Mol Oncol 2023;17(1):3–26. https://doi.org/10.1002/1878-0261.13308.

Related article

1. NOD2/CARD15 mutations in Polish and Bosnian populations with and without Crohn's disease: Prevalence and genotype-phenotype analysis

   Nermin N Salkic et al., BJBMS, 2015

Supplemental data

Supplemental data are available at the following link: https://www.bjbms.org/ojs/index.php/bjbms/article/view/13221/4077.